Journal of Fluids and Structures (2002) **16**(7), 989–1008
doi:10.1006/jfls.456 available online at http://www.idealibrary.com on IDEAL®

FLOW-INDUCED VIBRATION OF FREE EDGES OF THIN FILMS

Y.B. Chang

Department of Mechanical Engineering Technology, Oklahoma State University Stillwater, OK 74078, USA

AND

P.M. Moretti

School of Mechanical and Aerospace Engineering, Oklahoma State University Stillwater, OK 74078, USA

(Received 26 February 2001; and in final form 1 April 2002)

During manufacturing processes of thin materials such as paper, photographic film, and magnetic film, which are handled as continuous sheets and subjected to drying air-flows, the interaction of the air with the web can cause the free edges to vibrate violently. This phenomenon is related to the waving motion of a flag in the wind, except that the thin films under consideration are under tension in the direction of the air-flow or at right angles to it. A travelling-wave analysis was done based on incompressible potential-flow theory; the critical flow speed, wave speed, wavelength, and flutter frequency were predicted. A closed-form solution of the critical flow speed is suggested. Experiments were carried out with stationary thin films mounted in a wind tunnel where the direction of tension was perpendicular to the flow direction. It was shown that the analysis, which assumes that the film is infinitely long in the flow direction, could successfully predict the critical flow speed above which violent edge vibrations occur.

1. INTRODUCTION

1.1. Problem Definition

In manufacturing processes involving continuous sheets or webs of material, interaction of the material with the surrounding air dominates the out-of-plane dynamics of the web: the hydrodynamic mass effect (Lamb 1932) exceeds the mass of the sheet for all but the shortest wavelengths. If air is blown along the web for the purpose of drying, the web may become unstable and deflect out-of-plane. The present study investigates the stability limits when air blows from the center-line of the web towards the free edges.

1.2. Relevance

In papermaking, a sheet of paper 6–10 m in width is formed by removing excess water from slurry of fibers by mechanical means. The wet paper travels through a series of dryers 1 000–2 000 m/min, supported by felts. For effective drying of the fabric, the paper web is

0889-9746/02/070989 + 20 $35.00/0

often separated from the felts between drying rollers, as shown in Figure 1. The unsupported span occasionally breaks, resulting in the production loss while the machine is rethreaded. The break can often be traced back to violent vibrations of the paper edges.

The felt rollers are sometimes relocated such that the felts can give partial support to the paper span. However, in the wedge-shaped spaces near rollers, positive or negative pressures are developed due to the velocity of the webs and the rollers, causing the paper to separate from the felt. To reduce the separation, blow boxes, with slots along the full width of the web, blow drying air against the paper. Excess air departs through the sides of the machine, leading to a cross-machine direction (CMD) air-flow. Figure 2 is a simplified view of a moving web subjected to air flowing towards the edges. In real-world situations, the air-flow is not uniform and the flow field is three-dimensional.

While paper nonuniformity, tension fluctuations, and turbulence may all contribute to web breaks, we will demonstrate that a flow-induced instability is the fundamental cause of edge flutter. Increased machine speed and drying air-flow both increase aerodynamic effects and the risks of flutter, breaks, and downtime. Increased tension reduces flutter, but can itself be a cause of tearing. Gauging these trade-offs, maximizing productivity, and improving drying-air management, all require a theory for predicting the incidence of severe flutter.

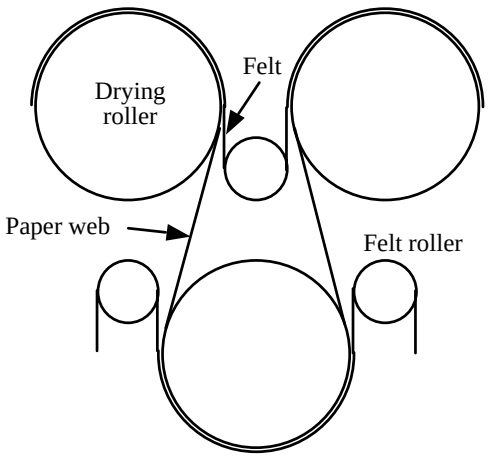

Figure 1. Paper web in dryer section.

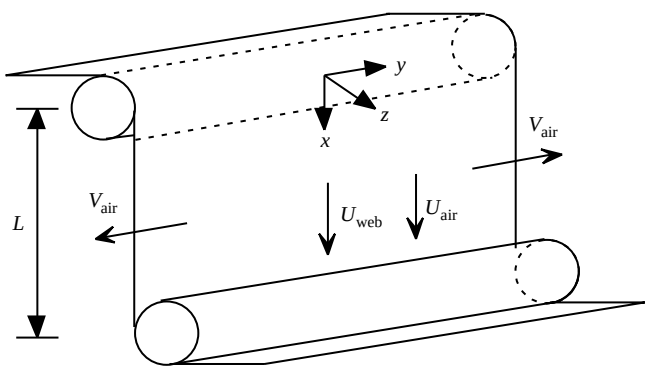

Figure 2. Simplified view of a moving web subjected to a flow field.

1.3. Background

A number of closely related flutter phenomena have been investigated in the past, as summarized below. The first two of them are typical problems observed in paper making or paper converting processes.

1.3.1. Flutter due to parallel flow

When the air-flow is parallel (i.e., machine direction or MD) to a long, narrow web (e.g., in the ink-drying section of printing plants), the governing equation for long-wave out-of-plane motions is similar in form to the thread-line equation (Moretti 1999)

$$A\frac{\partial^2 w}{\partial t^2} \pm 2B\frac{\partial^2 w}{\partial t \partial x} - C\frac{\partial^2 w}{\partial x^2} = F(t, x), \tag{1}$$

but the coefficient A includes both web mass and hydrodynamic inertia; the Coriolis coefficient B includes both web velocity and air velocity terms; and the apparent-tension coefficient C includes web, air, and tension terms (Chang *et al.* 1991). If B is negative, it can be made positive by choosing the x-coordinate direction appropriately; and the magnitudes of A and C can be brought to unity by rescaling the coordinates x and/or t, so that the equation reduces to

$$\ddot{w} + 2b\dot{w}' \mp w'' = f, \tag{2}$$

where $b = B\sqrt{|AC|}$. If the apparent-tension coefficient C is positive, the negative sign prevails for the third term, and the system is stable. Because of the mixed derivative, the fundamental free-vibration solution has the form (Chang & Moretti, 1991)

$$w^* = \sin(x^*)\cos\left(t^* + \frac{b}{\sqrt{1+b^2}}x^*\right), \tag{3}$$

where x^* and t^* are dimensionless.

However, if the air velocity is sufficient to make the apparent-tension-coefficient C negative, the positive sign prevails for the third term, and the solution is steadily divergent, with the web bulging towards positive or negative w. At even higher velocities, an oscillatory instability is observed (Chang *et al.* 1991).

1.3.2. Flutter due to cross-flow

When the air-flow is towards the edge of a wide web (i.e., in the CMD), the material velocity and the air velocity are at right angles to each other. Early experiments (Chang & Moretti 1992) used a stationary web. It was demonstrated that the web vibration is not due to random turbulence, but shows the well-defined critical velocity, characteristic of flutter phenomena. The stroboscopically observed waves travelled in the direction of the flow, and increased in amplitude towards the edge.

Further experiments were carried out with a moving web traversing a wind tunnel, with the upstream edge protected from the air-flow (Chang *et al.* 1999). Simultaneous laser vibrometer measurements at two points were correlated to obtain travelling-wave information (Moretti *et al.* 1994). At the velocities tested, air velocity effects dominated, relative to web-translation effects.

1.3.3. Flag flutter

Flag flutter is similar to the low-tension (i.e., slack edge) limiting case of edge flutter. Note, however, that there are several major differences between flag flutter and edge flutter. One major difference is that, for the edge flutter discussed in this paper, only the downstream

edge of the web is free while flags have three free edges. The air-flow around the two free edges along the flow direction has a significant effect on the dynamics of a flag. Even among the flag models, there are many major differences. Those study-models include cantilevered vertical plates that are clamped at the upstream top end and free on other three edges (Datta & Gottenberg 1975), cantilevered horizontal plates with three unconstrained edges (Yamaguchi *et al.* 2000a), membranes hanging vertically on piano wires with three unconstrained edges (Taneda 1968; Uno 1973), half-infinite plates with free trailing edges (Yamaguchi *et al.* 2000b), and a half-infinite membrane with free trailing edge and subjected to tension in the flow direction (Sparenberg 1962). Fairthorne (1930) demonstrated that the interaction of the air with the waving flag generates drag forces, and Thoma (1939) pointed out that the oscillatory motion of a flag creates intermittent tension due to the centrifugal forces on the leech edge of the flag.

1.3.4. Panel flutter

Aeroelastic panel flutter (Dowell 1966; Oyibo 1983) resembles web flutter, except for the greater importance of stiffness versus tension, the difference in typical boundary conditions, and, in the supersonic case, the shift from second-derivative-dependent pressure forces to first-derivative terms.

2. ANALYSIS

2.1. Study Model

The dynamics of a moving web is modelled as shown in Figure 3. The support rollers are modelled as infinite baffles perpendicular to the moving web, the web is assumed to be subjected to a uniform air-flow in the cross-direction moving from the center-line of the web to its free edges, and the effect of the air-flow in the machine direction is ignored.

2.2. Governing Equations

The governing equation of the out-of-plane motion of a translating web (thin and continuous material) is

$$m\left(\frac{\partial^2 w}{\partial t^2} + 2U_{\text{web}}\frac{\partial^2 w}{\partial t \partial x} + U_{\text{web}}^2\frac{\partial^2 w}{\partial x^2}\right) + \left(D_x\frac{\partial^4 w}{\partial x^4} + 2D_{xy}\frac{\partial^4 w}{\partial x^2 \partial y^2} + D_y\frac{\partial^4 w}{\partial y^4}\right)$$
$$-\left(T_x\frac{\partial^2 w}{\partial x^2} + 2T_{xy}\frac{\partial^2 w}{\partial x \partial y} + T_y\frac{\partial^2 w}{\partial y^2}\right) + p_+ - p_- = 0, \tag{4}$$

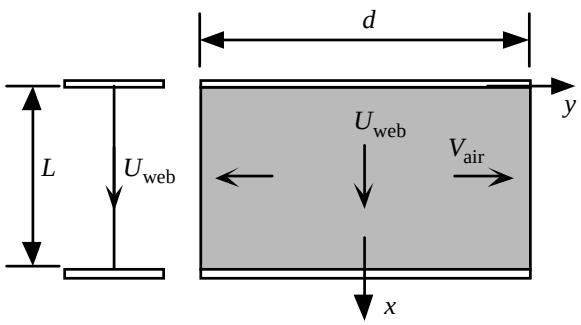

Figure 3. Schematic of the study model.

where (Graff 1975)

$$D_x = \frac{E_x h^3}{12(1 - v_x v_y)}, \quad D_y = \frac{E_y h^3}{12(1 - v_x v_y)} \quad \text{and} \quad D_{xy} = D_x v_y + \frac{G h^3}{6}. \tag{5}$$

As sketched in Figure 4, it is assumed that a travelling-wave-type flutter occurs along the flow direction (the y direction or CMD), the effect of the reflected wave at the downwind edge is negligible, the shape of web deflection along the longitudinal direction (machine direction) is $\sin(\pi x/L)$, and the wavelength is much smaller than the width of the web ($\lambda/d << 1$), and web tension is uniform. Under these assumptions the shape of web deflection can be expressed as

$$w = \hat{w} \sin\left(\frac{\pi x}{L}\right) e^{i(\omega t - ky)} = \hat{w} \sin\left(\frac{\pi x}{L}\right) e^{ik(ct - y)}. \tag{6}$$

If the wavenumber k is a complex number with positive imaginary component, the system is said unstable because the amplitude of the web increases with y; if the angular frequency ω is a complex number with negative imaginary component, the system is unstable because the wave amplitude increases with time without limit. It is assumed in this analysis that the wavenumber is a real number, but the angular frequency (and so the phase speed) can be a complex number. By substituting equation (6) into equation (4), we obtain

$$A \cdot \hat{w} e^{i(2\pi/\lambda)(ct - y)} \sin\frac{\pi x}{L} - i\left(2mU_{\text{web}}\frac{2\pi^2 c}{\lambda L} + 2T_{xy}\frac{2\pi^2}{\lambda L}\right)\hat{w} e^{i(2\pi/\lambda)(ct - y)} \cos\frac{\pi x}{L} - p_+ + p_- = 0, \tag{7}$$

where

$$A \equiv m\left(\frac{2\pi c}{\lambda}\right)^2 + \frac{mU_{\text{web}}^2 \pi^2}{L^2} - D_x\left(\frac{\pi}{L}\right)^4 - 2D_{xy}\left(\frac{2\pi^2}{\lambda L}\right)^2 - D_y\left(\frac{2\pi}{\lambda}\right)^4 - T_x\left(\frac{\pi}{L}\right)^2 - T_y\left(\frac{2\pi}{\lambda}\right)^2.$$

The aerodynamic pressure on the web is expressed by the Bernoulli equation,

$$p_\pm = -\rho \left[\frac{\partial \phi}{\partial t} + V_{\text{air}}\frac{\partial \phi}{\partial y}\right]_{z=0\pm}. \tag{8}$$

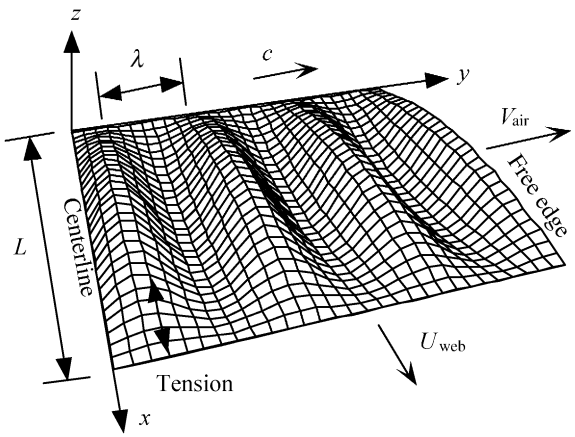

Figure 4. Assumed pattern of flutter.

The velocity potential should satisfy

$$\nabla^2\phi - \frac{1}{a^2}\left(\frac{\partial}{\partial t} + V_{\text{air}}\frac{\partial}{\partial y}\right)^2 \phi = 0. \tag{9}$$

2.3. Boundary Conditions

The boundary condition of the velocity potential on the web surface is

$$\left.\frac{\partial\phi}{\partial z}\right|_{z=0\pm} = \frac{\partial w}{\partial t} + V_{\text{air}}\frac{\partial w}{\partial y}, \quad 0 < x < L. \tag{10}$$

If the supports of the web are assumed to be infinite walls perpendicular to the web as shown in Figure 3, there must be no flow in the x direction (longitudinal or machine direction) at $x = 0$ and $x = L$. If we ignore the air-flow in the longitudinal direction (windage caused by the translational motion of the web), the condition for the velocity potential is

$$\frac{\partial\phi}{\partial x} = 0 \quad \text{for } x = 0 \quad \text{or } x = L. \tag{11}$$

2.4. Velocity Potential

The velocity potential should have the form

$$\phi(x, y, z, t) = \hat{\phi}(x, z)\, \mathrm{e}^{\mathrm{i}(2\pi/\lambda)(ct-y)}. \tag{12}$$

Substitution of equation (12) into equation (9) yields

$$\frac{\partial^2\hat{\phi}}{\partial x^2} + \frac{\partial^2\hat{\phi}}{\partial z^2} - \left(\frac{2\pi}{\lambda}\right)^2\left[1 - \left(\frac{V_{\text{air}} - c}{a}\right)^2\right]\hat{\phi} = 0. \tag{13}$$

Let $\hat{\phi}(x, z) = X(x)Z(z)$, then the above equation becomes

$$\frac{X''}{X} + \frac{Z''}{Z} - \left(\frac{2\pi}{\lambda}\right)^2\left[1 - \left(\frac{V_{\text{air}} - c}{a}\right)^2\right] = 0. \tag{14}$$

Let $X''/X = -r^2$. If we assume $r > 0$, the function X becomes $X = A_1\mathrm{e}^{\mathrm{i}rx} + A_2\mathrm{e}^{-\mathrm{i}rx}$. Furthermore, let $Z''/Z - q^2 = 0$, where

$$q^2 = r^2 + \left(\frac{2\pi}{\lambda}\right)^2\left[1 - \left(\frac{V_{\text{air}} - c}{a}\right)^2\right], \tag{15}$$

the real component of which is positive. The general solution to the equation $Z''/Z - q^2 = 0$ is $Z = A_3\mathrm{e}^{qz} + A_4\mathrm{e}^{-qz}$. For positive z, $Z = A_4\mathrm{e}^{-qz}$, so that $\hat{\phi}(x, z) = \mathrm{e}^{-qz}(A_1\mathrm{e}^{\mathrm{i}rx} + A_2\mathrm{e}^{-\mathrm{i}rx})$. By considering the boundary condition at $x = 0$ (which is $\partial\phi/\partial x = 0$), the velocity potentional is obtained to be $\hat{\phi}(x, z) = A\mathrm{e}^{-qz}\cos(rx)$. At $x = L$, $\partial\phi/\partial x = 0$, so that $\sin(rL) = 0$. From which, $r_n = n\pi/L$, where n is a positive integer. Equation (15) now becomes

$$q_n = \frac{\pi}{L}\left\{n^2 + \left(\frac{2L}{\lambda}\right)^2\left[1 - \left(\frac{V_{\text{air}} - c}{a}\right)^2\right]\right\}^{1/2}. \tag{16}$$

The profile of the velocity potential can be rewritten as $\hat{\phi}(x,z) = \sum_{n=0}^{\infty} A_n e^{-q_n z} \cos(n\pi x/L)$, from which

$$\left.\frac{\partial \hat{\phi}(x,z)}{\partial z}\right|_{z=0} = -\sum_{n=0}^{\infty} A_n q_n \cos\frac{n\pi x}{L}. \tag{17}$$

From equations (6), (10) and (12), the boundary condition of the velocity potential on the web surface can be written as

$$\left.\frac{\partial \hat{\phi}(x,z)}{\partial z}\right|_{z=0} = -\mathrm{i}\frac{2\pi}{\lambda}(V_{\mathrm{air}} - c)\hat{w}\sin\frac{\pi x}{L}. \tag{18}$$

Therefore,

$$\sum_{n=0}^{\infty} A_n q_n \cos\frac{n\pi x}{L} = \mathrm{i}\frac{2\pi}{\lambda}(V_{\mathrm{air}} - c)\hat{w}\sin\frac{\pi x}{L}. \tag{19}$$

The coefficients A_n are evaluated using the Fourier transform formula as

$$A_o = \mathrm{i}\frac{4(V_{\mathrm{air}} - c)\hat{w}}{\lambda q_o}, \tag{20}$$

and if $n \geq 1$,

$$A_n = -\mathrm{i}\frac{8(V_{\mathrm{air}} - c)\hat{w}}{(n^2-1)\lambda q_n}$$
$$\text{for even } n, \quad \text{and } A_n = 0 \text{ for odd } n. \tag{21}$$

The velocity potential can be written as

$$\phi(x,y,z,t) = \mathrm{i}\frac{4(V_{\mathrm{air}} - c)\hat{w}}{\lambda}\left[\frac{1}{q_o} - \sum_{n=1}^{\infty}\frac{2}{(4n^2-1)q_{2n}} e^{-q_{2n}z}\cos\frac{2n\pi x}{L}\right] e^{i(2\pi/\lambda)(ct-y)}. \tag{22}$$

2.5. Aerodynamic Loading

The air pressure on the positive z-side surface is determined by substituting equation (22) into the Bernoulli, equation (8), yielding,

$$p_+ = -\frac{8\pi\rho(V_{\mathrm{air}} - c)^2\hat{w}}{\lambda^2}\left[\frac{1}{q_o} - \sum_{n=1}^{\infty}\frac{2}{(4n^2-1)q_{2n}}\cos\frac{2n\pi x}{L}\right] e^{\mathrm{i}(2\pi/\lambda)(ct-y)}. \tag{23}$$

The air pressure on the other side of web is $p_- = -p_+$, so that $-p_+ + p_- = -2p_+$.

2.6. Out-of-plane Motion of the Web

From equations (7) and (23), we obtain

$$A\sin\frac{\pi x}{L} - \mathrm{i}\left(2mU_{\mathrm{web}}\frac{2\pi^2 c}{\lambda L} + 2T_{xy}\frac{2\pi^2}{\lambda L}\right)\cos\frac{\pi x}{L} + \frac{16\pi\rho(V_{\mathrm{air}} - c)^2}{\lambda^2}\left[\frac{1}{q_o} - \sum_{n=1}^{\infty}\frac{2\cos(2n\pi x/L)}{(4n^2-1)q_{2n}}\right] = 0. \tag{24}$$

If we multiply each term with the assumed mode shape $\sin(\pi x/L)$ and integrate over $0<x<L$, the above equation becomes

$$A+\frac{64}{\lambda^2}\rho(V_{\text{air}}-c)^2\left[\frac{1}{q_o}+\sum_{n=1}^{\infty}\frac{2}{(4n^2-1)^2q_{2n}}\right]=0. \tag{25}$$

Note that the Coriolis term $\partial^2 w/\partial t\,\partial x$ and the term $\partial^2 w/\partial x\,\partial y$ dropped out by forcing the symmetric deflection shape $\sin(\pi x/L)$ to be applied. Define the reference speed as $c_o^2 \equiv \pi^2 D_x/mL^2$, and introduce the following nondimensional parameters: $\bar{c}\equiv c/c_o$, $\Lambda \equiv \lambda/2L$, $M \equiv 2\rho L/\pi\, m$, and $\bar{T}\equiv T_x L^2/\pi^2 D_x$. Then equation (25) becomes

$$\bar{c}^2-B+\frac{8}{\pi L}M(\bar{V}_{\text{air}}-\bar{c})^2\left[\frac{1}{q_o}+\sum_{n=1}^{\infty}\frac{2}{(4n^2-1)^2q_{2n}}\right]=0, \tag{26}$$

where

$$B=(1+\bar{T}-\bar{U}_{\text{web}}^2)\Lambda^2+\frac{2D_{xy}}{D_x}+\frac{D_y}{D_x}\Lambda^{-2}+\frac{T_y}{T_x}\bar{T}. \tag{27}$$

The cross-flow velocity V_{air} is much lower than the sonic speed a for typical paper mills, and the experiment to be discussed later was done in the range of $V_{\text{air}}/a<0{\cdot}1$. The wave speed does not exceed the air speed. Therefore, $(V_{\text{air}}-c)/a\ll 1$ so that

$$q_{2n}\simeq\frac{\pi}{L}\sqrt{4n^2+\Lambda^{-2}}\quad\text{for } n\geq 0. \tag{28}$$

With this condition, equation (26) becomes

$$\left(1+\frac{8sM}{\pi^2}\right)\bar{c}^2-\frac{16sM}{\pi^2}\bar{V}_{\text{air}}\bar{c}+\frac{8sM}{\pi^2}\bar{V}_{\text{air}}^2-B=0, \tag{29}$$

where

$$s=\Lambda+\frac{2}{9\sqrt{4+\Lambda^{-2}}}+\frac{2}{225\sqrt{16+\Lambda^{-2}}}+\ldots\simeq\Lambda+\frac{2}{9\sqrt{4+\Lambda^{-2}}}. \tag{30}$$

The solution to the quadratic algebraic equation (29) is

$$\bar{c}=\frac{8sM\bar{V}_{\text{air}}\pm\pi\sqrt{-8sM\bar{V}_{\text{air}}^2+(\pi^2+8sM)B}}{\pi^2+8sM}. \tag{31}$$

The system becomes unstable when the phase speed is a complex number because of its negative imaginary component.

2.7. Critical Conditions

The critical flow speed is determined from the condition at which the term inside the square-root sign in equation (31) becomes zero, i.e., for

$$\bar{V}_{\text{air}}^2=\left(1+\frac{\pi^2}{8sM}\right)B=\left(1+\frac{\pi^2}{8sM}\right)\left[(1+\bar{T}-\bar{U}_{\text{web}}^2)\Lambda^2+\frac{2D_{xy}}{D_x}+\frac{D_y}{D_x}\Lambda^{-2}+\frac{T_y}{T_x}\bar{T}\right]. \tag{32}$$

The nondimensional phase speed of flexural waves in the web at and above the critical condition is the real part of $\bar{c}$, that is $\bar{c}_R=8sM\bar{V}_{\text{air}}/(\pi^2+8sM)$. There are an infinite number of critical flow speeds, corresponding to the infinite number of possible wavelengths. We need to find the values of Λ at which the critical flow speed becomes minimum. It is more appropriate to define the term "critical flow speed" as the minimum

possible value of flow speed which satisfies equation (32). The term "critical" will be used accordingly in the remaining parts of this paper. Flutter frequencies at, and higher than, the critical flow speed are obtained by

$$\bar{f} \equiv f\frac{2L}{c_o} = \frac{\bar{c}_R}{\Lambda} = \frac{8sM}{(\pi^2 + 8sM)\Lambda}\bar{V}_{\text{air}}. \tag{33}$$

It must be noted that the flutter frequency is not linearly proportional to the flow speed. The variable s in equation (33) is a function of wavelength, which in turn depends on flow speed. In the supercritical range of flow speed, both the wavelength and the flutter frequency are double-valued functions of flow speed.

2.8. Approximation of the Critical Flow Speed: Closed-Form Solution

It is not convenient to use equation (32), because it requires us to find the value of the critical wavelength, i.e., we need to find the condition at which the flow speed expressed by equation (32) becomes minimum. This section discusses an approximate method of determining the critical flow speed. The resulting equation of the critical flow speed is a closed-form solution.

The central region of a stretched free span of web is under compressive cross-stress. The web can be corrugated due to buckling due to a compressive loading. Shelton (1991) showed that the wavelength of the corrugation is $\lambda/2L = [1 + 12\sigma_x(1 - \nu^2)(L/h)^2/\pi^2 E]^{-1/4}$, that is,

$$\Lambda = (1 + \bar{T})^{-1/4}, \tag{34}$$

where it was assumed that the material is isotropic so that the subscript on bending stiffness was dropped. If we assume that the wavelength of a fluttering web is the same as that predicted by the above equation, equation (32) becomes an explicit equation for the nondimensional critical flow speed.

3. EXPERIMENTS AND COMPARISON WITH THEORY

3.1. Experimental Set-Up

A web material was mounted in a subsonic wind tunnel as shown in Figure 5. The web was in stationary position ($U_{\text{web}} = 0$). The wind tunnel is a suction-type, open-circuit design. The test section is 0·622 m (24·5 in) wide and 0·413 m (16·25 in) high. The flow speed can be as high as about 70 m/s, but the experiment was done mostly at speeds lower than 30 m/s. The downwind edge of the tested web was free, while all the other sides were fixed. Web tension was applied in the cross-flow direction to simulate the machine-direction tension. For uniform tension distribution, the upwind edge area of the web had holes and parallel cuts, and the upwind clamp was released and fastened again each time the tension was changed. One type of paper and three types of plastic webs were tested. Test variables included web material (mass density, modulus of elasticity, thickness), web tension, and flow speed. For paper web, the effect of web length (flow-direction dimension, b) was also examined. Straight lines were drawn on the web, 25·4 mm apart in both tension and flow directions, for better observations of web motion.

Modulus of elasticity of the paper web was measured by a vibration testing. A strip of paper was attached to a rigid steel structure near the ceiling, and tension was applied and adjusted by a mass (steel disks). The mass was impacted in the vertical direction, and its vibration was measured by a proximity sensor. The modulus of elasticity could be

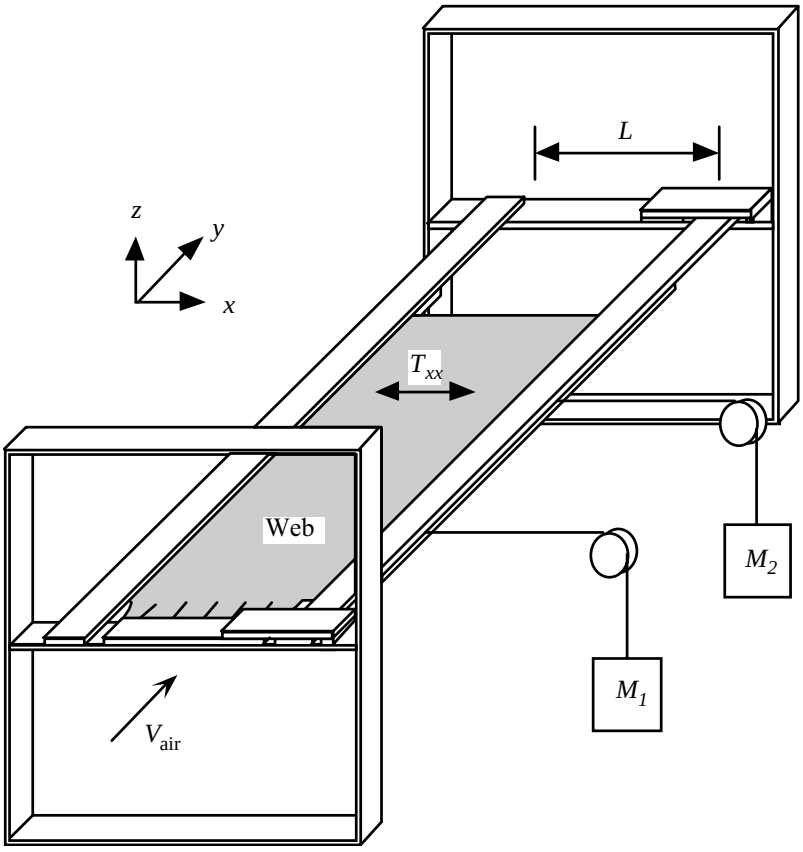

Figure 5. Schematic of the test setup mounted in a wind tunnel.

calculated from the equation of natural frequency, $f_n = \sqrt{EA/mL}/2\pi$, where E is the modulus of elasticity, A the cross-sectional area of the strip, L the length of the strip, and m the mass of the disks. The test was repeated for various values of mass. The modulus of elasticity of plastic webs was determined with the web mounted in the wind tunnel by measuring the amount of stretch at various loads. The amount of stretch was large enough for measuring the strain with a ruler with a reasonable accuracy. Material properties of the tested webs are summarized in Table 1.

We tried to measure web deflection using an optical sensor. The sensor had a rectangular rod shape with a cross-section of 6×19 mm. After the first flow test, we abandoned the use of the optical sensor because it affected web behavior; the downwind edge deflected towards the sensor and fluttered severely in the entire range of flow speed. Instead, we used a stroboscope to find the flutter patterns, the frequencies, and the amplitudes. This was not an accurate method of determining the flutter amplitude, but it worked reasonably well for the determination of the critical flow speed because the flutter amplitude changed drastically when the flow speed was near the critical value.

3.2. Observations

As the flow speed was increased from zero, the downwind free edge of the web started to vibrate randomly with small amplitudes. The amplitude grew with flow speed, and above a

TABLE 1

Properties of web materials and test conditions

	Paper	Plastic 1	Plastic 2	Plastic 3
m (kg/m^2)	0·058	0·023	0·120	0·240
E (MPa)	6800	50	50	50
L (m)	0·223	0·223	0·223	0·223
b (m)	0·30, 0·38, 0·46	0·46	0·46	0·46
h (μm)	76	20	102	203
T (N/m)	9–70	35–70	18–70	9–70

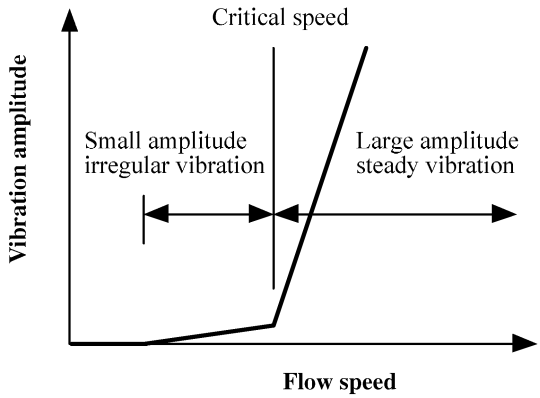

Figure 6. Typical amplitude response.

critical value of air speed the vibration became violent and steady, as indicated in Figure 6. We could determine the critical flow speed by measuring vibration amplitude or by detecting the oscillation frequency. In most cases, the transition occurred so suddenly that the critical flow speed could be determined with little uncertainty even if a crude method was used to measure the vibration amplitude. The transition from erratic vibration to steady vibration made it possible to determine the threshold condition by measuring the frequencies. Once the web became unstable, the flutter frequency tended to increase with flow speed.

The observed vibration was in the form of waves travelling in the flow direction. With the stroboscope frequency a little lower than the flutter frequency, the waves appeared to move downstream; while with higher strobe-light frequency, the waves appeared to move upstream. Therefore, the waves were propagating in the direction of the air-flow. Even near the downwind free edge, the waves appeared to move in the flow direction only; but the amplitude at the downwind edge was much larger than at the upstream one.

The observed vibration of the downwind free edge (and any straight line in the tension direction) was of normal mode. Up to a certain value of the flow speed in the supercritical condition, the zero-node pattern was observed (Figure 7). When the flow speed is much higher than the critical value, the downwind edge vibrated with higher modes (more nodes and higher frequencies). For given flow speed, only a single mode vibration occurred in steady manner, and the pattern of deflection could be observed very clearly.

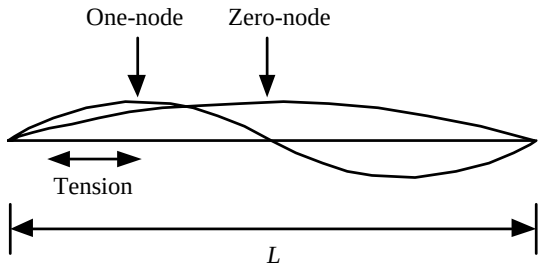

Figure 7. Vibration modes of the free edge.

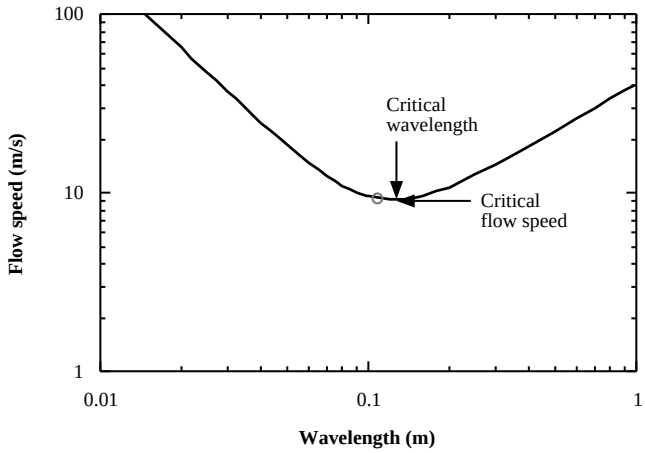

Figure 8. Wavelength and critical flow speed for paper at $T = 17{\cdot}2$ N/m: (○), approximation; (—), full equation.

In most cases, the critical speed of air-flow increased with web tension. The effect of web length (flow-direction dimension, b), however, was not evident in the range of test conditions. We could not separately test the effects of mass density and bending rigidity of the web because it was impossible to change one of them without affecting the other.

3.3. Wavelength at Critical Flow Speed

We attempted to observe the wavelengths near the critical flow speeds. Unlike the measurement of critical flow speeds and flutter frequencies, however, measurement of wavelength could not be done accurately enough to discuss the data in detail. Figure 8 illustrates the theoretical relationship between the critical flow speed and the wavelength for two different values of web tension for the paper web tested. The solid line is from equation (32) without any assumption for the wavelength; the symbol is from the same equation but with the critical wavelength determined by equation (34). In both cases it was assumed that $T_y = 0$. It is seen that the simple, closed-form solution yields nearly the same result as the equation which requires a more complicated procedure for determining the critical condition. Figures 9–11 are for plastic films of three different thicknesses. The common shape of the curves implies that, near the critical condition, even a large error in the prediction of the critical wavelength causes a relatively small error in the critical flow speed.

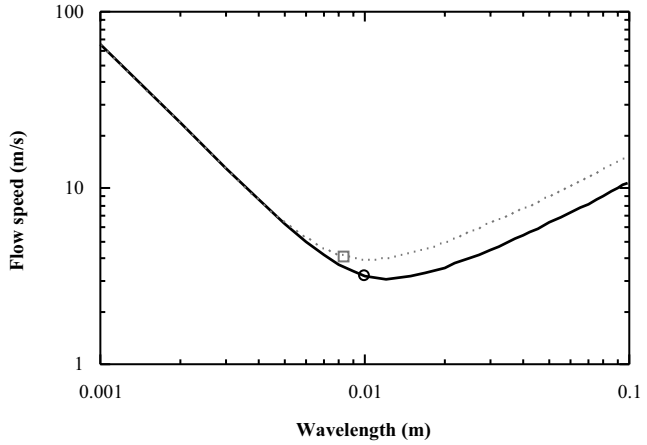

Figure 9. Wavelength and critical flow speed for Plastic 1: ○, $T = 34{\cdot}3$ N/m, approximation; □, $T = 68{\cdot}6$ N/m, approximation; —, $T = 34{\cdot}3$ N/m, full equation; ·····, $T = 68{\cdot}6$ N/m, full equation.

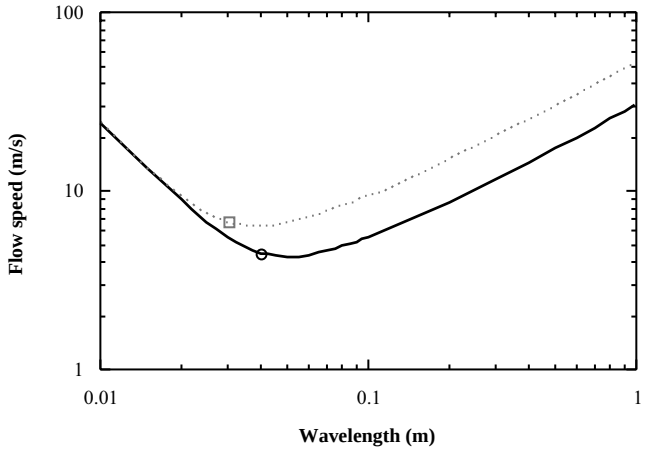

Figure 10. Wavelength and critical flow speed for Plastic 2: ○, $T = 17{\cdot}2$ N/m, approximation; □, $T = 51{\cdot}5$ N/m, approximation; —, $T = 17{\cdot}2$ N/m, full equation; ·····, T = 51·5 N/m, full equation.

3.4. Critical Flow Speed

The measured values of the critical flow speed for the paper web are compared with the predicted values in Figure 12. The solid line in the figure is based on equation (32) without any assumption for the wavelength, and the dotted line is based on the wavelength given by equation (34). The two prediction curves fall on each other for the paper web tested. For the plastic materials tested, the two equations predict slightly different values of the critical flow speeds, but the differences are not significant (Figure 13). In general, the theories tend to underpredict the critical flow speed.

All test data are plotted against the approximation equation in nondimensional form in Figure 14. It appears that even though the theory underpredicts the critical flow speeds, the errors are not very large and the predicted trend is the same as measured.

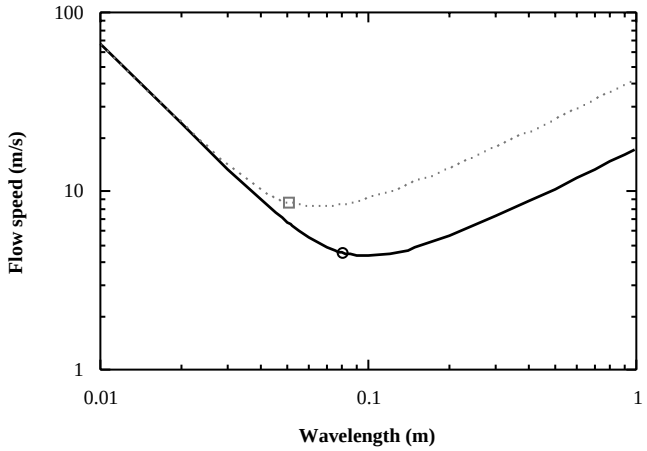

Figure 11. Wavelength and critical flow speed for Plastic 3: ○, $T = 8{\cdot}6$ N/m, approximation; □, $T = 51{\cdot}5$ N/m, approximation; —, $T = 8{\cdot}6$ N/m, full equation; ·····, $T = 51{\cdot}5$ N/m, full equation.

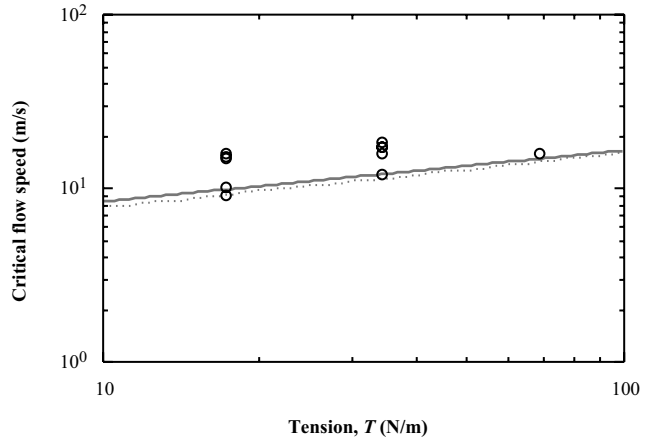

Figure 12. Critical flow speed for paper: ○, measured; —, approximation; ·····, full equation.

3.5. Flutter Frequency

The measured dominant flutter frequencies of the paper web at $T = 17{\cdot}2$ N/m are compared with the predicted values in Figure 15. Note that, in this figure and other frequency plots, only the values near the experimental critical conditions are shown; the simple stability analysis in this paper is not suitable for predicting behavior of the web in post-critical conditions. The measured flutter frequency tended to increase with the flow speed. Note that the theory indicates that, at each flow speed, there are two possible values of flutter frequency. The left end of the curve indicates the critical condition: the critical flow speed and the corresponding value of frequency. It is not certain whether the scatter in the data in Figure 15 indicates experimental errors or two different trends implied by the theory. Unless we can relate each data point to one of the upper and lower prediction lines, we cannot plot a nondimensional frequency curve similar to that for critical flow speed

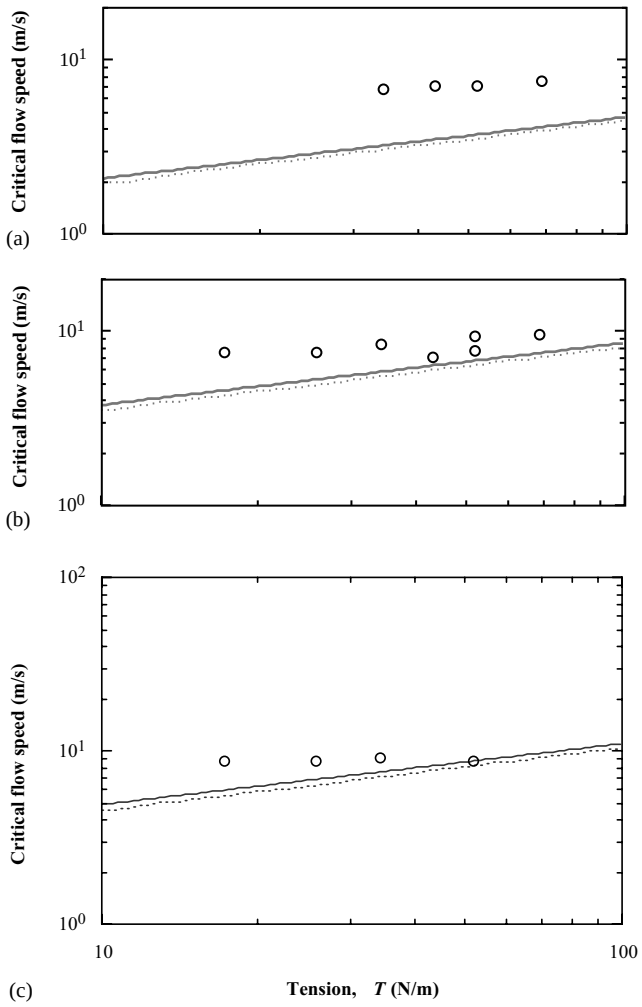

Figure 13. Critical flow speed for (a) Plastic 1, (b) Plastic 2, (c) Plastic 3: ○, measured; —, approximation; ·····, full equation.

shown in Figure 14. Additional frequency data are compared with theory in Figure 16. For Plastic 1 which is 20 mm in thickness, the measured values of the frequency fall between the upper and lower prediction curves (Figure 17). For thicker plastic films, it appears that the measured frequencies are close to the upper prediction curves (Figures 18 and 19).

4. DISCUSSION

One of the assumptions in the analysis is that the flow-direction dimension of the web is much larger than the wavelength. In our experiments, $3 \leq b/\lambda \leq 8$ for paper, and $5 \leq b/\lambda \leq 18$ for plastic webs. These values might not be large enough to justify the assumption and could be one possible cause of errors. The flow boundary conditions at

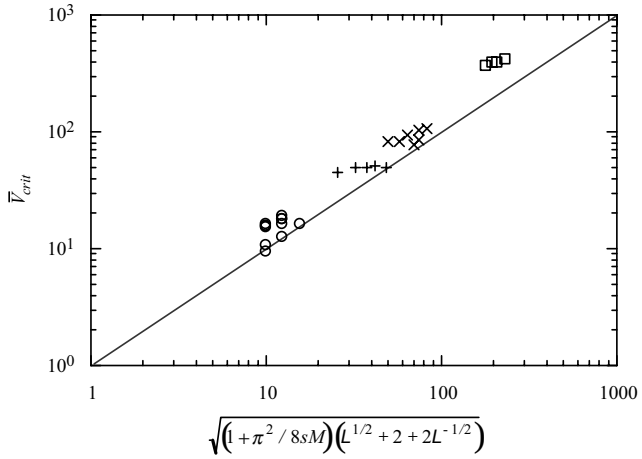

Figure 14. Predicted and measured nondimensional critical flow speeds: ○, Paper; □, Plastic 1; ×, Plastic 2; +, Plastic 3; —, Prediction.

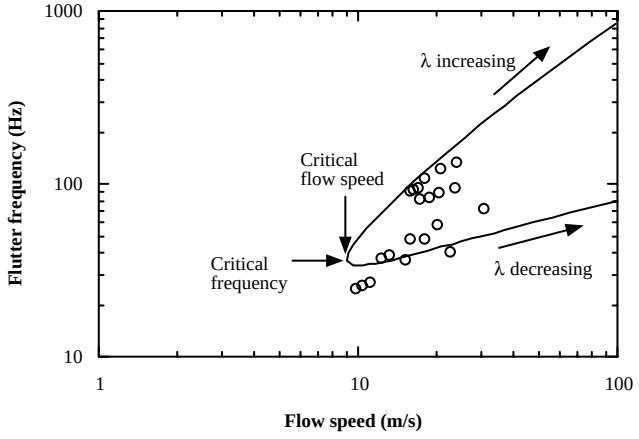

Figure 15. Flutter frequency of Paper for $T = 17{\cdot}2\,\mathrm{N/m}$: ○, measured; —, predicted.

$x = 0$ and $x = L$ of the test set-up are not the same as those of the analytical model. This difference might be another cause of discrepancy between the theory and the experiments.

The frequency of vortex-shedding from the web-holding jig was always much higher than the observed flutter frequency. Therefore, the observed flutter phenomenon was not due to the vortex shedding of the air flow.

Our experimental observations indicated that edge flutter of flexible materials such as paper and plastic films is not due to the fluid–structure interaction at the trailing free edge. Using strobe light, edge flutter was seen to be a travelling wave phenomenon, and waves in the flow direction dominate the phenomenon. Therefore, for typical web handling applications, the Kutta condition is not as important as in some other fluid–structure interaction phenomena where the fluid flow near the trailing edge plays a crucial role.

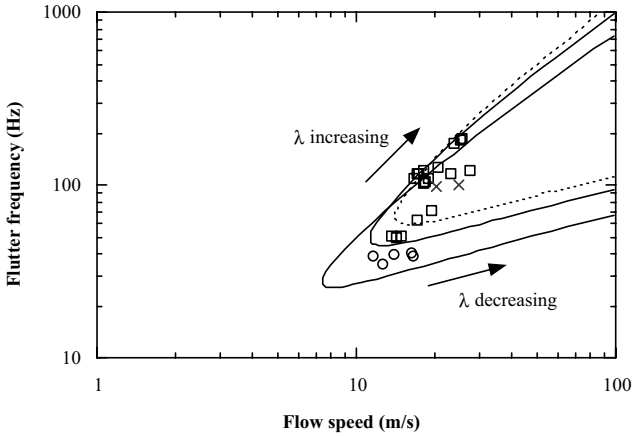

Figure 16. Flutter frequency of Paper: ○, $T = 8{\cdot}6$ N/m, measured; □, $T = 34{\cdot}3$ N/m, measured; ×, $T = 68{\cdot}6$ N/m, measured; —, $T = 8{\cdot}6$ N/m, predicted; —, $T = 34{\cdot}3$ N/m, predicted; ·····, $T = 68{\cdot}6$ N/m, predicted.

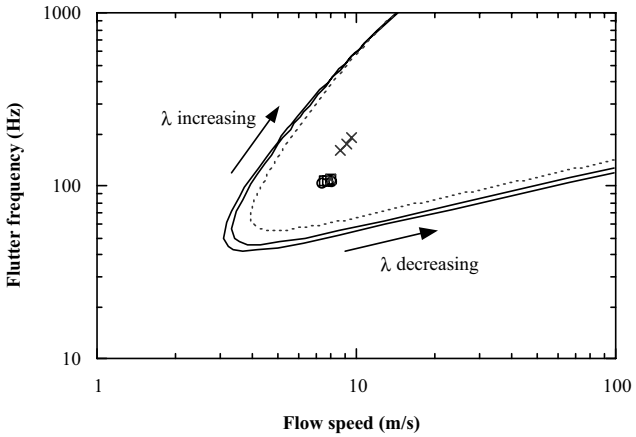

Figure 17. Flutter frequency of Plastic 1: ○, $T = 34{\cdot}3$ N/m, measured; □, $T = 42{\cdot}9$ N/m, measured; ×, $T = 68{\cdot}6$ N/m, measured; —, $T = 34{\cdot}3$ N/m, predicted; —, $T = 42{\cdot}9$ N/m, predicted; ·····, $T = 68{\cdot}6$ N/m, predicted.

5. CLOSING REMARKS

The study of edge flutter expands previous studies of two-dimensional waves to a more realistic three-dimensional problem. The theory and the experiments clearly showed that there is an inherent mechanism of web instability, contrary to the belief of many engineers who thought that edge flutter occurs mainly due to turbulence of the air-flow.

Experimental results indicate that the analysis underpredicts the critical flow speed. However, it appears that the theory can be used as a means of predicting the possibility of harmful edge-flutter problems. The simple, closed-form solution of the critical flow speed suggested in this paper will be very useful for this purpose.

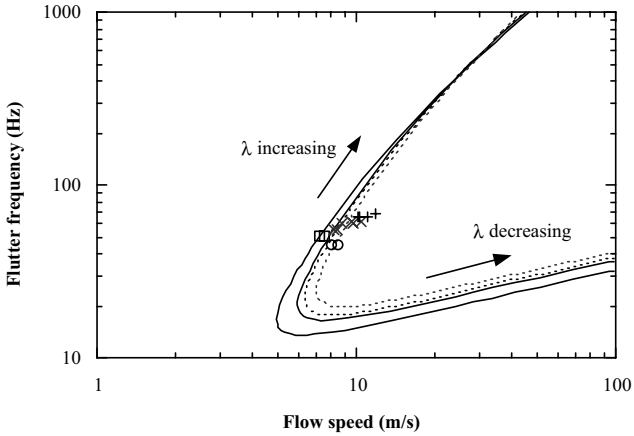

Figure 18. Flutter frequency of Plastic 2: ○, $T = 25{\cdot}7$ N/m, measured; □, $T = 42{\cdot}9$ N/m, measured; ×, $T = 51{\cdot}5$ N/m, measured; +, $T = 68{\cdot}6$ N/m, measured; —, $T = 25{\cdot}7$ N/m, predicted; — $T = 42{\cdot}9$ N/m, predicted; —-, $T = 51{\cdot}5$ N/m, predicted; ·····, $T = 68{\cdot}6$ N/m, predicted.

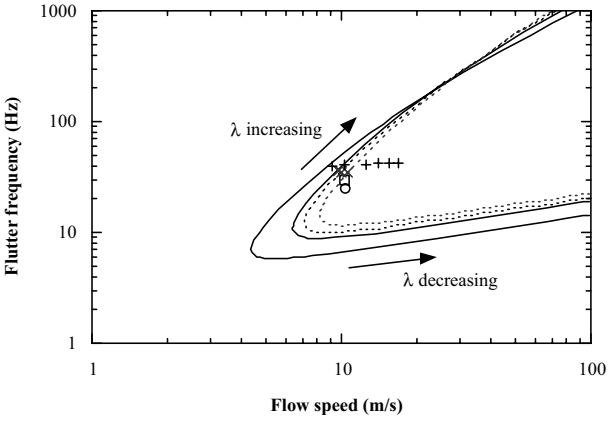

Figure 19. Flutter frequency of Plastic 3: ○, $T = 8{\cdot}6$ N/m, measured; □, $T = 25{\cdot}7$ N/m, measured; ×, $T = 34{\cdot}3$ N/m, measured; +, $T = 51{\cdot}5$ N/m, measured; —, $T = 8{\cdot}6$ N/m, predicted; —, $T = 25{\cdot}7$ N/m, predicted; —-, $T = 34{\cdot}3$ N/m, predicted; ·····, $T = 51{\cdot}5$ N/m, predicted.

ACKNOWLEDGEMENTS

The authors are grateful to the Web Handling Research Center at Oklahoma State University and its consortium members for the financial support for this research.

REFERENCES

CHANG, Y. B., CHO, C. H. & MORETTI, P. M. 1999 Edge flutter. In *Proceedings of the ASME Noise Control and Acoustics Division*, ASME NCA-Vol. 26 pp. 413–423.

CHANG, Y. B., FOX, S. J., LILLEY, D. G. & MORETTI, P. M. 1991 Aerodynamics of moving belts, tapes, and webs. In *Machinery Dynamics and Element Vibrations*, ASME DE-Vol. 36 pp. 33–39; presented at ASME Thirteenth Biennial Conference on Mechanical Vibration and Noise, Symposium on Dynamics of Axially Moving Continua, Miami, Florida, Sept. 22-25, 1991.

Chang, Y. B. & Moretti, P. M. 1991 Interaction of fluttering webs with surrounding air. *TAPPI Journal* **74,** 231–236.
Chang, Y. B. & Moretti, P. M. 1992 An experimental study on edge flutter in webs. In *Web Handling*, ASME AMD-Vol. 149, pp. 67–78; presented at ASME Winter Annual Meeting, Anaheim, Calif., Nov. 11, 1992.
Datta, S. K. & Gottenberg, W. G. 1975 Instability of an elastic strip hanging in an airstream. *Journal of Applied Mechanics* **42,** 195–198.
Dowell, E. H. 1966 Flutter of infinitely long plates and shells—Part I: Plate. *AIAA Journal* **4,** 1370–1377.
Fairthorne, R. A. 1930 Drag of flags. ARC Reports and Memoranda No. 1345.
Graff, K. F. 1975 *Wave Motion in Elastic Solids*. New York: Dover Publications.
Lamb, H. 1932 *Hydrodynamics*. New York: Dover Publications.
Moretti, P. M. 1999 *Modern Vibrations Primer*, pp. 302-303. Boca Raton, FL: CRC Press.
Moretti, P. M., Chang, Y. B. & Vedula, K. 1994 Vibration intensity measurement of fluttering webs by laser-doppler sensors. *SPIE Proceedings Series, Vibration Measurements by Laser Techniques: Advances and Applications*, Vol. 2358, pp. 409–420.
Oyibo, G. A. 1983 Unified aeroelastic flutter theory for very low aspect ratio panels. *AIAA Journal* **21,** 1581–1587.
Shelton, J. J. 1991 Machine direction troughs in web spans and corrugations in wound rolls. Internal Report of the Web Handling Research Center at Oklahoma State University.
Sparenberg, J. A. 1962 On the waving motion of a flag. *Proceedings of Netherlands Academy of Sciences* **B65,** 378–392.
Taneda, S. 1968 Waving motions of flags. *Journal of the Physical Society of Japan* **24,** 392–401.
Thoma, D. 1939 Das Schlenkernde Seil (The Oscillating Rope). *Zeitschrift fuer Angewandte Mathematik und Mechanik* **19,** 320–321.
Uno, M. 1973 Fluttering of flexible bodies. *Journal of the Textile Machinery Society of Japan* **19,** 103–109.
Yamaguchi, N., Sekiguchi, T., Yokota, K., & Tsujimoto, Y. 2000a Flutter limits and behavior of a flexible thin sheet in high-speed flow ii: experimental results and predicted behaviors for low mass ratios. *ASME Journal of Fluids Engineering* **122,** 74–83.
Yamaguchi, N., Yokota, K. & Tsujimoto, Y. 2000b Flutter limits and behaviors of a flexible thin sheet in high-speed flow i: analytical method for prediction of the sheet behavior. *ASME Journal of Fluids Engineering* **122,** 65–73.

APPENDIX: NOMENCLATURE

a	speed of sound in air
b	flow-direction dimension of tested web, $b = d/2$
c	phase speed of waves in the web
c_o	reference speed, $c_o \equiv \pi\sqrt{D_x/mL^2}$
D	flexural rigidity of web, $D \equiv Eh^3/12(1-\nu^2)$
d	width of web, $d = 2b$
E	modulus of elasticity of web
f	flutter frequency
G	shear modulus of web
h	thickness of web
i	$\sqrt{-1}$
k	wavenumber of the y direction (cross-machine direction or flow direction) waves
L	web span (distance between two supports)
M	mass ratio, $M \equiv 2\,\rho L/\pi m$
m	mass per unit area of web
p	aerodynamic pressure on the web surface (subscript $\pm$ indicates upper or lower surface)

U_{web}	translation speed of web
$\bar{U}_{\text{web}}$	nondimensional speed of web, $\bar{U}_{\text{web}} \equiv U_{\text{web}}/c_o$
T	tension (tensile force per unit width of web) (subscript x or y indicates direction)
T_m	apparent tension, $T_m \equiv T_x - mU_{\text{web}}^2$
$\bar{T}$	tension parameter, $\bar{T} \equiv T_m L^2/\pi^2 D_x$
t	time
V_{air}	flow speed in the y direction (cross-machine direction)
$\bar{V}_{\text{air}}$	nondimensional flow speed, $\bar{V}_{\text{air}} \equiv V_{\text{air}}/c_o$
w	out-of-plane deflection of web (in the z direction)
$\dot{w}$	vibration velocity of web
$\hat{w}$	out-of-plane deflection coefficient of web
x	longitudinal direction (machine direction) coordinate
y	cross-machine direction (flow direction) coordinate
z	out-of-plane direction (perpendicular to web surface) coordinate
Λ	nondimensional wavelength, $\Lambda \equiv \lambda/2L$
λ	wavelength of the y direction waves
v	poisson's ratio of web material
ρ	density of air
ϕ	velocity potential
σ	stress (subscript x or y indicates direction)
ω	angular frequency

Subscripts

crit	critical value
I	imaginary component
R	real component
x	machine direction
y	cross-machine direction
$+$	upper surface of web ($z > 0$)
$-$	lower surface of web ($z < 0$)

Superscript

*	normalized coordinate